Solvent Mediated Inclusion of Metal Oxide Into Block Copolymer Nanopatterns: Mechanism of Oxide Formation Under UV-Ozone Treatment

Tandra Ghoshal, John O'Connell, Christophe Sinturel, Pascal Andreazza, Justin D. Holmes, Michael A. Morris

Graphical Abstract:

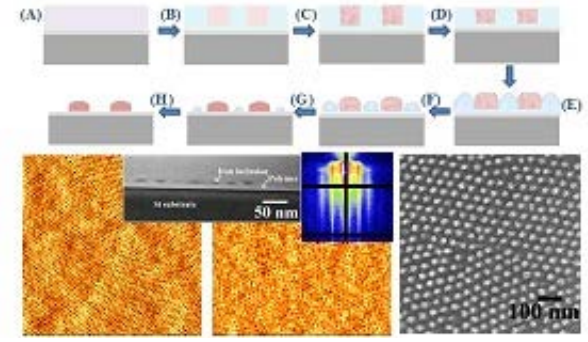

Solvent Mediated Inclusion of Metal Oxide Into Block Copolymer Nanopatterns: Mechanism of Oxide Formation Under UV-Ozone Treatment

Tandra Ghoshal,[†*] John O'Connell,[‡] Christophe Sinturel,[₸] Pascal Andreazza,[₸] Justin D. Holmes,[‡] Michael A. Morris[†*]

[†]School of Chemistry, AMBER and CRANN, Trinity College Dublin, Dublin, Ireland

[‡]Department of Chemistry and Tyndall National Institute, University College Cork, Cork, Ireland

[₸]Centre National De La Recherche Scientifique, Universite D'orleans, Orleans, France

[*] Corresponding Author:

Prof. Michael A. Morris

Tel: +353 1 896 3089

Fax: +353 1 896 3089

E-mail: morrism2@tcd.ie

And

Tandra Ghoshal

Tel: + 353 21 490 2911

Fax: +353 21 427 4097

E-mail: g_tandra@yahoo.co.in

ABSTRACT: Uniform, periodic and ordered iron oxide nanopatterns can be generated by selective metal ion inclusion into microphase separated polystyrene-b-poly(ethylene oxide) (PS-b-PEO) block copolymer (BCP) thin films. After solvent mediated metal ion inclusion into the PEO block, an ultraviolet-Ozone (UVO) treatment was used to remove the polymer and oxidize the metallic ions to their oxides. This paper provides an in-depth study of the UVO processing steps as a function of exposure time. Surface wettability, topography, morphology, compositional and interfacial changes were analysed by contact angle measurement, microscopic and spectroscopic techniques through the UVO treatment. It was found that the UVO treatment initially cross-links the polymer network followed by oxidation and removal of the polymer simultaneously. It was also found that if short UVO exposure times are used, a post calcination treatment can be used to generate similar patterns. The iron oxide nanopatterns created due to strong coordination bond between metallic ions and free electron pairs of O atoms in the PEO and these interactions are responsible for the final pattern mimicking the original self-assembled BCP morphology. The film thicknesses, surface roughness, the size/shape of the iron oxides and patterns, the amount of residual polymers were also investigated regarding the UVO exposure time.

KEYWORDS: Block Copolymers, oxides, nanoparticles, patterns, UV/Ozone, XPS

1. INTRODUCTION

The nanopatterning of materials on surfaces has become increasingly important in the field of electronics, optics, photonics, biology, electrochemistry, and electromechanics.[1-2] The increasing costs of conventional UV lithography coupled to continued reduction of feature size, has led to self-assembly becoming a potential means of delivering nanometer dimensioned pattern fabrication strategies to industry.[3-4] In recent years, di-block copolymer (Di-BCP) self-assembly has been intensively studied for potential integration into nanopatterning nanoelectronic fabrication techniques.[5] Numerous publications describe work where a self-assembled di-BCP film act as an on-chip etch mask or a template and material patterns can be produced by selective removal of one copolymer block (and subsequent pattern transfer to the substrate) or selective inclusion of chemical components to a chosen block (and subsequent processing).[6-10] We have pioneered the formation of inorganic oxide nanodot and nanowire patterns using selective inclusion of inorganics into modified microphase separated cylindrical phase PS-b-PEO thin films.[11-16] These studies focussed on development of the methodology - BCP ordering, inclusion techniques and post-processing. However, for further development and application it is necessary to provide a clear understanding of mechanism(s) of the process so that the methods used can be properly optimised.

In our previous work we largely used ultraviolet-ozone (UVO) treatment to convert the precursor infiltrated into BCP nanopatterns into an oxide nanofeature arrangement mimicing the original BCP morphology. UVO treatment is an alternative to e.g. oxidative plasma treatments as it avoids high kinetic energy particles that might damage the film through the process of polymer removal and metal precursor oxidation.[17] UVO is highly effective in removing the BCPs and can be conducted under ambient conditions ensuring the equipment is cost-effective.[18] In order to understand the mechanism of inclusion and contribute to a detailed understanding of the overall process, it is necessary to investigate the UVO technique in detail.

This paper reports on the oxidization of the carbonaceous materials and inorganic precursors whilst enhancing the material-substrate adhesion as a function of exposure time. The interaction between metal, polymer and substrate is studied in terms of surface chemistry, topography, wettability and morphology as a function of UVO time. The studies will lead to a greater understanding of the changes in structure and chemistry that occur on the modified polymer-inorganic surfaces.

2. Materials and Methods

2.1. Preparation of iron oxide nanodot arrays by block copolymers. The PS-b-PEO Di-BCP was purchased from Polymer Source and used without further purification (number-average molecular weight, M_n, PS = 42 kg mol^{-1}, M_n, PEO = 11.5 kg mol^{-1}, the polydispersity was 1.07). Single crystal B doped P type silicon (100) wafers with a 10 nm adventitious silica layer were used as a substrate. Substrates were cleaned by ultrasonication in acetone and toluene for 30 minutes in each solvent and dried under nitrogen. PS-b-PEO was dissolved in toluene to yield 1 wt% polymer solution and aged for 12 h at room temperature. The PS-b-PEO thin film was formed by spin coating (3000 rpm for 30 s). The films were exposed to toluene/water (50:50, v/v, 1.5 ml/1.5 ml) vapour placed at the bottom of a closed vessel kept at 50 °C for 1 h to induce necessary chain mobility and promote microphase separation. Partial etching and domain modification of PEO was carried out by ultrasonication of the films at 40^0 C for 16 h in anhydrous alcohol. The films were then removed and dried. For the fabrication of iron oxide nanodots, Iron (III) nitrate nonahydrate ($Fe(NO_3)_3$,$9H_2O$) was dissolved in ethanol (1% w/w) and spin-coated onto the substrate. UVO was used to oxidize the precursor and remove polymer. UVO treatment was carried out for different time (5, 10, 15, 20, 25, 30, and 45 min and 1, 1.5, 2, 2.5 and 3 h) to study the formation of iron oxide and removal of polymer.

2.2. Characterizations. In the UV/Ozone treatment, ozone, an active oxidizing agent, is generated in situ from atmospheric oxygen by exposure to 185 nm UV light. The ozone produced subsequently photo dissociates into molecular oxygen and atomic oxygen upon exposure to 254 nm light. The latter specie reacts with the polymer to form free radicals and activated species that eventually remove organic portions of the polymer in the form of carbon dioxide, water, and a small amount of volatile organic compounds. Surface morphologies were imaged by atomic force microscopy (AFM, Park systems, XE-100) in tapping mode and scanning electron microscopy (SEM, FEI Company, FEG Quanta 6700 and Zeiss Ultra Plus). The film thicknesses were measured by optical ellipsometer (Woolam M2000) and electron microscopy. The ordering of the film was investigated by grazing incidence small angle X-ray scattering (GISAXS). The measurements were performed with a diamond light source at beamline I07 (SI 8065) with monochromatized X-rays (λ = 0.15 nm) having grazing incident angle ranging from 0.09 to 0.20^0. Samples were prepared for transmission electron microscopy (TEM) cross sectional imaging with an FEI Helios Nanolab 600i system containing a high resolution Elstar™ Schottky field-emission SEM and a Sidewinder FIB column. A 40 nm carbon layer was deposited to enhance the contrast and to distinguish between iron compounds and the interfaces. TEM was carried out on a JEOL 2100 or an FEI Titan. Surface wettability was evaluated with an electronic goniometer from Ossila Ltd. Contact angle θ (°) measurements were performed based on the sessile drop method. 5 µl drops of deionised water were deposited on the samples with a micropipette. Averages of three independent measurements were registered for each sample and characterized angle. X-Ray photoelectron spectroscopy (XPS) experiments were conducted on a Thermo K-alpha machine with Al K_α X-ray source operating at 72 W.

3. RESULTS AND DISCUSSION

3.1. BCP template preparation for iron precursor inclusion. The BCP studied here has PEO as the minority, cylinder forming block. Our understanding of this system has been developed earlier[12, 15-16] and optimum ordering of the BCP with a perpendicular orientation of PEO was achieved under toluene/water mixed solvent vapour at 50 °C for 1 h. Figure 1a shows the representative tapping mode AFM image of the PS-b-PEO after the solvent vapour exposure indicating well-defined periodic, microphase separated arrangements across the substrate with no indication of film de-wetting. The average center to center distance between adjacent microdomain is 42 nm with a PEO cylinder diameter is 19.3 nm (PEO cylinders are the darker AFM features). The film thickness measured by ellipsometry was 40 nm. Ethanol treatment is critical to properly include inorganic compound into the PEO domain as has also been described.[12, 15-16] This treatment partially degrades or modifies the PEO but crucially decreases the PEO cylinder volume to allow solvent inclusion and swelling. Note, we use the terms nanoporous and pores to describe this structure but this does not imply complete removal of PEO. The periodicity and cylinder dimensions are unchanged (within experimental error) after ethanol treatment as revealed by AFM image in Figure 1b. No thickness change was observed as measured by ellipsometry. The polymer nanoporous template formed is monolayer and well adhered to the substrate surface as previously reported. Figure 1c represents the AFM image of the iron precursor loaded BCP template after spin coating with 0.4 wt% precursor-ethanol solution. The concentration of iron precursor was optimized to achieve an optimum loading and avoid deposition onto the PS or pattern degradation.

3.2. Morphological evolution of precursor-BCP template as a function of UVO processing time.

3.2.1. Topographic AFM imaging. The iron precursor-BCP template was subjected to UVO treatment for different times to oxidize the precursor and remove polymer. The surface-interfacial morphological and structural changes and compositions were studied through the

UVO treatment time (Figures 1(d-l) are the relevant AFM topographical images). The modified BCP film retains the original morphology etc. after 5 min UVO treatment (Figure 1d). Pattern degradation, decreased periodicity, increased surface roughening and thickness variations are observed with longer UVO processing times of 10 min (Figure 1e) and 15 min (Figure 1f). It is apparent that the darker spots typical of the cylinders are growing and merging suggesting that reaction is taking place around the edge of the cylinders and could be catalysed in nature due to the presence of iron. There is little sign of the formation of iron oxide nanodots and the periodicity expected of them and strongly suggests that nanodot formation occurs below the surface of the film. The surface roughening observed suggests periodicity in the polymer component is lost and intermediate reaction products are distributed across the surface. UVO processing times of 20 min (Figure 1g), 25 min (inset of Figure 1g) and 30 min (Figure 1h) begin to exhibit enhanced periodicity and white spots appear typical of the iron oxide nanodots. This suggest the polymer film height is decreasing to a value similar to the height of the iron oxide nanodots. The nanodots appear to grow in size through the increased exposure but this may be a tip convolution effect as the pattern is becoming topographically patterned as the polymer is consumed at a faster (catalytic enhancement) rate around the cylinders. Note that film thickness undulation is still seen and clearly the rate of polymer oxidation varies across the substrate. AFM images in Figures 1(i-l) depicts well-ordered periodically spaced nanoparticle arrays with UVO processing time of 45 min, 1h, 1h 30 min and 2h respectively. At these longer times, ordered large area nanoparticle arrays were realized with uniform size/shape and their arrangement mimics that of the original BCP patterns. The oxidation process is clearly advancing and the remaining polymer is removed. The average diameters of the nanoparticles increased with increasing UVO processing time whereas centre to centre spacing (42 nm) remained unchanged. The cylinder diameter increase may indicate a nucleation and growth process is occurring. The final diameter of the nanoparticles was 22 ±

3 nm which is slightly greater than the original PEO cylinder width. This confirms conversion of the metal precursor to oxide which leads to lateral growth of the nanoparticles by oxidation process and removal of any residual PEO cylinders as well as PS matrix. The average nanodot heights were between 6-8 nm as measured by ellipsometry for 2 h UVO time. The density of the nanodots on the substrate was measured at approximately 1.1 x 10^{11} nanodots cm^{-2}.

As expected, the average thicknesses of the film decreases with UVO exposure time. For 5 and 10 min UVO time, the measured film thicknesses are 37 and 34 nm i.e. minimal removal of the polymers. Film removal with time is not linear or homogeneous and the film roughens. For 15 min exposure time, the thickness measured varied between 20-26 nm for various locations. Average thicknesses were 16, 14 and 10 nm for the films exposed for 20, 25 and 30 min respectively. After 45 min, the final thickness of 6-8 nm was achieved. No noticeable changes were realized with further increasing the UVO time to 1 h and above.

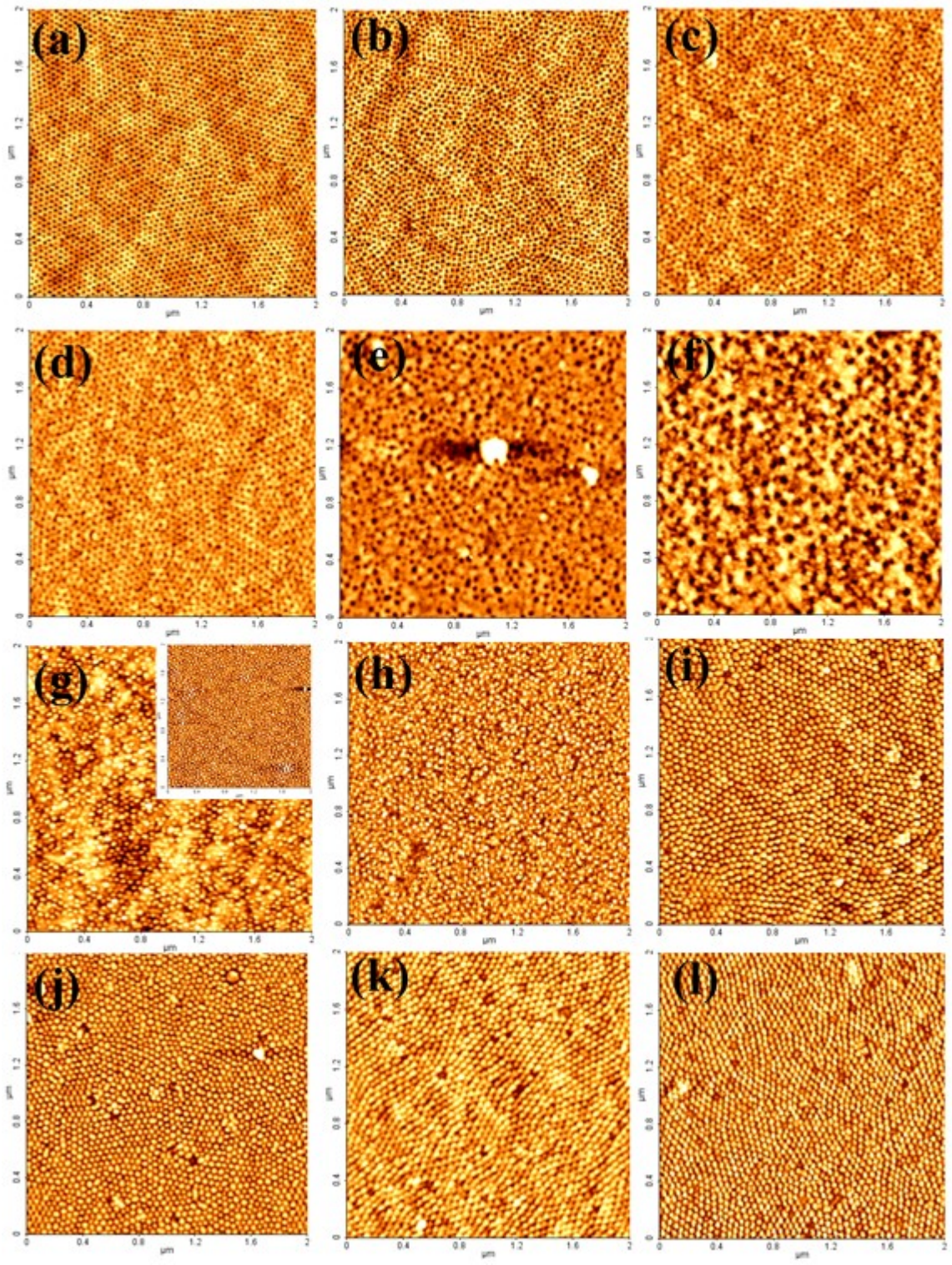

Figure 1. Tapping mode AFM images of the PS-b-PEO film (a) after the solvent vapour exposure, (b) after the ethanol treatment and (c) after spin coating the iron precursor. The iron oxide-BCP film for different UVO exposure time (d) 5 min, (e) 10 min, (f) 15 min, (g) 20 min, (inset of g) 25 min, (h) 30 min, (i) 45 min, (j) 1h, (k) 1h 30 min, (l) 2h.

Figure 2 shows the variation of film thickness with the UVO exposure time. This shows a sharp decrease of thickness for the UVO time to 30 minutes which become almost constant for the UVO time period between 45 min to 3 h. This decrease preliminary measures the removal of polymers but a slight increase in the thickness occur due to oxygen addition during oxidation of the precursor. Thus a combination effect of etching of polymers and precursor oxidation is responsible of the thickness variation.

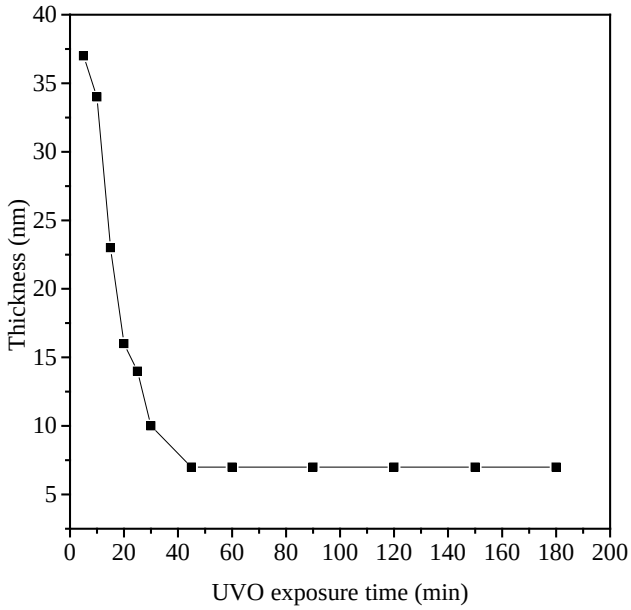

Figure 2. Variation of film thickness with UVO exposure time.

3.2.2. Top-down SEM. SEM, provides complimentary information to AFM because the signal arises from deeper within the film due to the finite escape depth of the secondary electrons. SEM images in Figures 3(a-j) represent the top-down images with increasing UVO processing time. Similar to the corresponding AFM image, periodic nanopatterns were seen across the substrate for 5 mins UVO time (Figure 3a). A higher magnification image (inset of Figure 3a) shows interconnection between pores are starting to form consistent with a catalytic mechanism. There are also white rings around pores in various locations and this may be due to slight overfilling or swelling of a few pores during infiltration. Film decomposition is seen

more clearly after 10 min UVO times (Figure 3b). Here, there are regions of decreased ordering. However, greater periodicity is observed compared to the corresponding AFM image suggesting the disorder seen in AFM is at the surface. This is confirmed in Figure 3c (15 mins UVO exposure) where iron oxide nanodots related to oxide formation are clearly visible (and were not by AFM). This suggests the iron oxide dots form close to the substrate-polymer interface. That they are not seen after 5 and 10 mins UVO exposure by SEM does suggest they are not formed as distinct particles at lower exposure times and remain as ions in the polymer pattern. Figures 3(d-g) show the development of the periodic nanodots within the polymer matrix for UVO exposure times of 20, 25, 30 and 45 min respectively. The nanodots appear to increase in diameter with time during the treatments as was seen by AFM. The nanoparticles are well separated from each other with the approximately the expected center-to-center spacing. Figures 3(h-j) describes periodic nanoparticles arrays for the UVO time of 1 h, 1 h 30 min and 2 h respectively. The polymer matrix layer is still present for 1 h UVO treatment and the contrast enhancement with processing time indicates the formation of oxide phase and removal of any residual polymers. Well defined, hexagonally arranged iron oxide nanoparticle arrays is generated for 1 h 30 min and 2 h processing time.

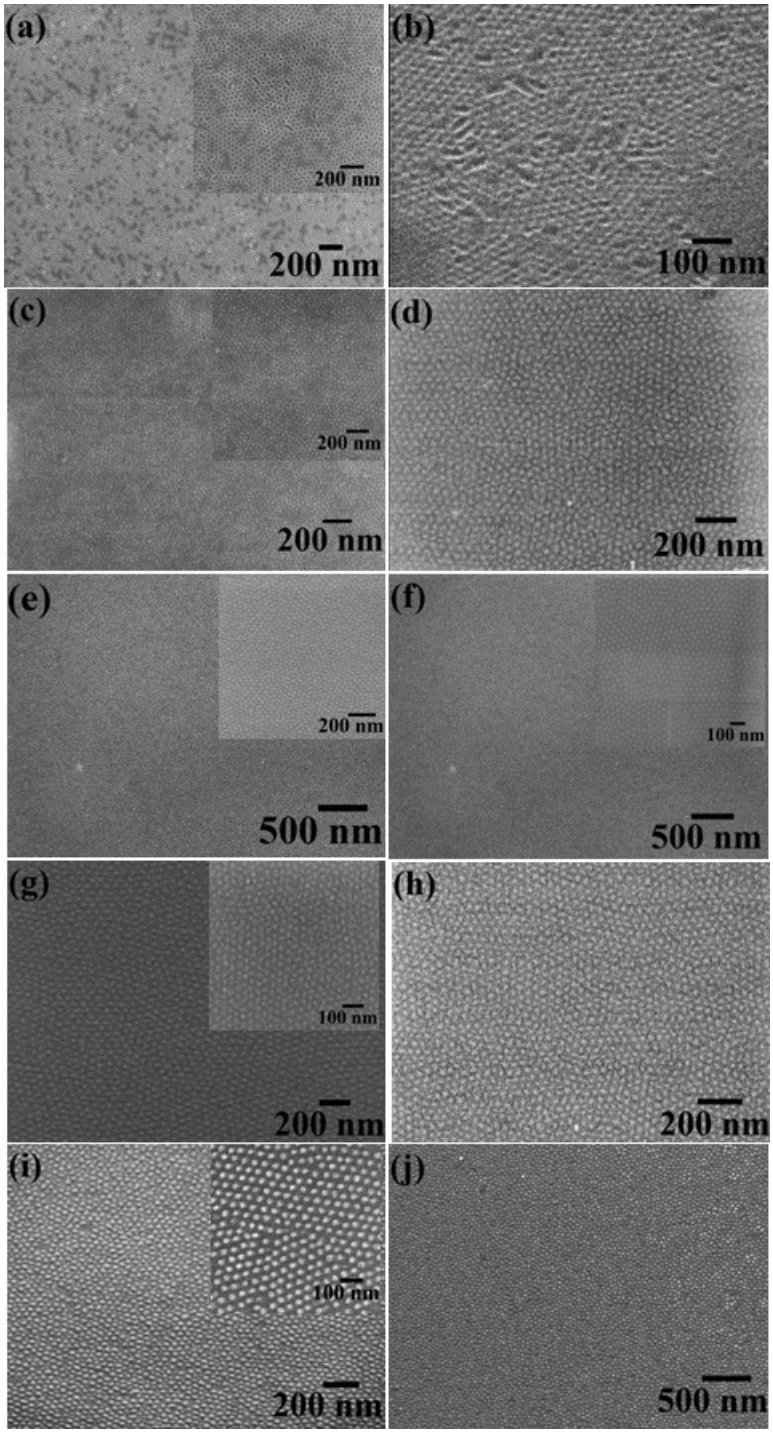

Figure 3. SEM images of the iron oxide-BCP film for different UVO exposure time (a) 5 min, (b) 10 min, (c) 15 min, (d) 20 min, (e) 25 min, (f) 30 min, (g) 45 min, (h) 1h, (i) 1h 30 min, (j) 2h.

3.2.3. Investigation of ordered periodic structure by GISAXS. AFM and SEM characterisation provide local ordering of the microdomains and as seen here is not consistent over the film area. X-ray characterization provides data across macroscopic length scales and can provide additional insight to the decomposition mechanism. Therefore, GISAXS was used to characterize the precursor loaded films as a function of UVO exposure. Figures 4(a-e) shows GISAXS (total external reflection mode) data for UVO processing time of 5, 10, 15, 20 and 45 min respectively. The critical angle of silicon was determined to be 0.2° from X-ray reflectivity data and this angle was used to ensure surface sensitivity. The images shown in Figure 4 represent reflections along the q_y scattering vector. For 5 min UVO exposure (Figure 4a), higher order scattering peaks can be clearly seen indicating a highly ordered, periodic structured film in agreement with AFM and SEM data.

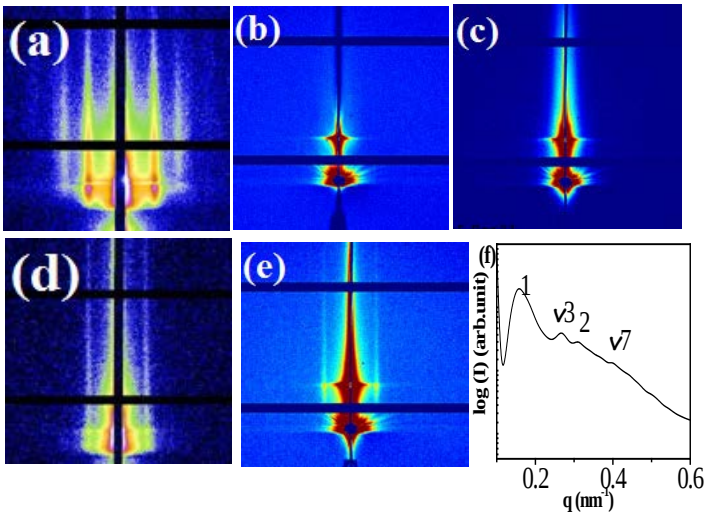

Figure 4. GISAXS 2D scattering spectra for UVO processing time of (a) 5 min, (b) 10 min, (c) 15 min, (d) 20 min and (e) 45 min respectively. (f) q_y line scan profile for 45 min UVO exposure time.

No clear scattering features were observed for 10 and 15 min UVO time confirming the disorder structure across the film surface as discussed above (Figures 4b and c respectively). The ordered arrangement reappears after 20 min UVO exposure as seen in Figure 4d and becomes more prominent after a 45 min UVO processing period (Figure 4e). From the detailed q_y line scan profile, the first order peak is observed at $q_y = 0.0149$ Å^{-1}, which corresponds to a microdomain spacing 42 nm (for 45 min processing time) consistent with the AFM and SEM results (Figure 4f). The hexagonal packing of the nanoparticles is confirmed by the relative peak positions of higher order reflections with respect to the first peak position, yielding the expected values 1, √3, 2 and √7.

3.2.4. Surface and interface study by cross-sectional TEM and EDAX mapping. Additional detail on the structural arrangement and location of precursor and the mechanism of iron oxide particle formation were obtained from TEM cross-sections. No interfacial cracks etc. at the interface of the film occurred during FIB processing, reflecting the adhesion and structural integrity of the film. Figures 5a and b shows FIB thinned TEM images for the 5 min UVO treated film. Lower magnification image (Figure 5a) reflects the inclusion of iron ions into the BCP templates as a darker contrast can be seen throughout the film surface. Higher magnification image (Figure 5b) clearly indicate a periodic arrangement of regions of darker contrast that can be associated with contrast caused by iron inclusion. The iron appears to be both within the cylinder structure and on top of the film surface (4-5 nm layer). This arrangement can be confirmed by the STEM image shown in the inset of Figure 5b (iron - lighter contrast). The data suggest that during the ethanol treatment, some of the PEO is distributed across the PS. This causes during the ethanol treatment for the formation of BCP template as reported previously.[16] The chemical structures of PEO monomers [(CH_2CH_2O)-] and ethanol molecules (H-CH_2CH_2O-H) are similar and it is asserted that during ethanol treatment, PEO chains are surrounded by ethanol molecules and becomes a miscible solution

because of very low PEO concentration allowing strong chemical interactions resulting in reaction and polymer degradation. When the BCP film was removed from the solution and dried at room temperature, the PEO molecules would prefer to segregate from the solution but cannot because those PEO monomers and ethanol molecules cannot distinguish from each other, as a result, the PEO chains are frustrated and have no choice to form a PEO-ethanol layer on top of the film surface. The diameter and depth of the cylinders are ~ 20 nm and 12 nm respectively and they are 42 nm apart. The cylinder containing film appears to be supported on a 9 nm polymer layer at the interface. This is most likely to be PS material as no iron appears to be present. These data clearly confirm selected inclusion into the PEO component. High resolution EDAX mapping confirms the elemental composition and the distribution of Fe, O and Si component shown in Figure 5c. The Fe map shows a homogeneous distribution of Fe within the nanopores and on top of the film surface. The O and Si maps confirm the presence of oxides on the film and passive layer of the substrate. The O layer across the substrate surface underneath the BCP film corresponds to 10 nm adventitious silica layer on top of the Si used as substrate. After 10 min UVO treatment (Figure 5d), a change occurs. The cylinder containing region of the film thins (4-5 nm) and the contrast due to iron increases (at both surface and in the cylinders) suggesting that as PEO is removed by the etch and that the iron increases in concentration in the remaining PEO. Figures 5e and f shows the TEM images for 30 min UVO treated films. A dramatic change occurs in this time period and the formation of iron oxide materials on the surface of the film can be seen with loss of the PS wetting layer (particles are now seen at the native oxide film above the silicon) and most of the other polymer materials. The iron oxide material is 3-4 nm nanodots of base diameter ~ 18 nm. The sudden change in structure suggests a change in mechanism. It is proposed that at some critical concentration of iron in the PEO block, that iron oxide particles nucleate. These catalyse the UVO oxidation of the polymer causing rapid loss of PEO and the PS wetting layer. With further

increase of UVO processing time (1 h and 1 h 30 mins, Figures 5g and 5i any remaining BCP template disappears and the diameter of iron oxide nanoparticles increases (~ 20 nm) while centre-centre spacing remain unchanged (Figures 5(g-i)). For 2h 30 min UVO time, higher magnification image shows hemispherical shape of the iron oxide particles with the measured thickness and diameter of ~ 5 nm and 20 nm respectively (Figure 5i).

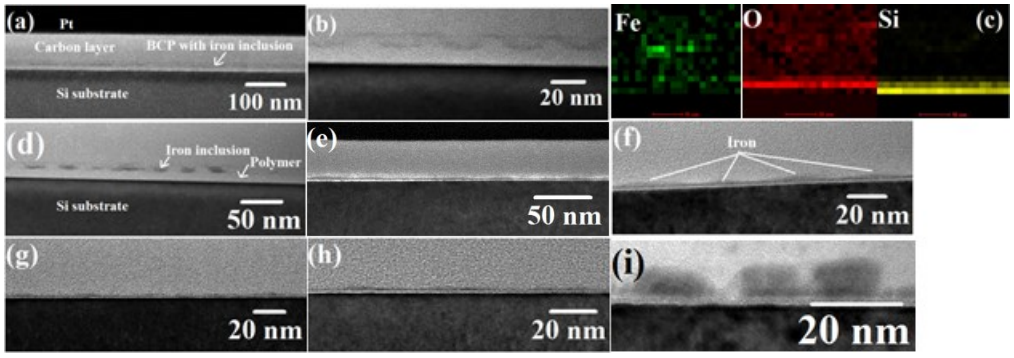

Figure 5. (a, b) FIB thinned TEM images and (c) EDAX mapping for Fe, O and Si after 5 min UVO exposure time. Similar data following UVO exposure times of (d) 10 min, (e, f) 30 min, (g) 1h, (h) 1h 30 min and (i) 2h 30 min.

3.2.5. Compositional analysis by XPS. Whilst the data in Figures 1-4 discuss structural changes, to understand the mechanism of the UVO treatment, the chemical decomposition of the film needs to be detailed. Hence, XPS analyses were performed for precursor loaded films with varying UVO treatment time. Figure 6a shows a typical survey spectrum indicating presence of expected elements, Si, O, Fe and C for all the samples. Table 1 shows the XPS derived composition for the scans taken after the UVO treatments. The intensities for the C1s peaks decreases with the UVO exposure consistent with removal of the polymer. Correspondingly, Fe2p peak intensities increase and their shapes become more defined with

time. High resolution C1s spectra reveal progressive chemical changes in the polymer as it is removed. Four carbon species are observed as illustrated in Figure 6b. The C1s spectra for all the samples processed between 5-45 min attributed to carbon from the aromatic ring of PS (**C**-$(C,H)_{arom}$) at 284.9 eV (overlapping with the adventitious C1s signal at 285.0 eV), carbon from the aliphatic backbone of PS (**C**-$(C,H)_{aliph}$) at 285.2 eV, carbon involved in an ether link (**C**-O-**C**) from PEO at about 286.5 eV.[19-20] The C-O-C component only comes from the PEO block and the rest of the carbon to the PS blocks. It can be from the data that all of the carbon peaks decrease between 5-45 min as material is removed and the pores broaden and merge consistent with the AFM and SEM results. The PS and remaining PEO are then removed more slowly before after 1.5 h, the peak shape begins to resemble single peak at 285.0 eV typical of adventitious carbon.

Fe 2p core level spectrum recorded after UVO treatment for different time (Figure 6c) two peaks associated with Fe $2p_{3/2}$ at 711.7 eV and Fe $2p_{1/2}$ at 725.4 eV are seen. These are broadened due to the existence of Fe^{+2} and Fe^{+3} ions. The Fe $2p_{3/2}$ binding energies (BEs) for Fe^{+2} and Fe^{+3} were determined by curve-fitting using Gaussian-Lorentzian line shapes. The measured Fe $2p_{3/2}$ BEs are 710.8 eV (assigned to Fe^{+2}) and 714.6 eV (Fe^{+3}) consistent with literature values.[21] The relative intensities of these features varied as a function of UVO exposure time (5 min – 1 h 30 min) which is listed in Table 1. The relative atomic concentration of Fe^{+2} was higher than Fe^{+3} for the UVO exposures of 5-30 minutes. Thereafter, the concentrations of Fe^{+3} increased due to further oxidation and reached a Fe^{+3}/ Fe^{+2} ratio ~ 2:1 for the UVO time of 2 h 30 min suggesting the formation of Fe_3O_4 phase.

Table 1: Elemental composition from XPS spectra with UVO processing time

UVO time	Si	O	C	Fe	Fe^{2+}	Fe^{3+}
5 min	2	58	38.4	1.6	52	48
10 min	3.7	62.4	32.2	1.7	56	44
15 min	11.3	59.1	24.4	5.2	63	37
20 min	36.6	29.3	21.7	12.4	67	33
25 min	44.2	26	15.8	14	67	33
30 min	44.3	31.3	9.2	15.2	60	40
45 min	44.6	31.3	8.5	15.6	53	47
1 h	45	33.4	6.2	15.4	50	50
1 h 30 min	41.2	37.3	6	15.5	45	55
2 h	38.8	39.6	6.1	15.5	39	61
2 h 30 min	38.2	40.2	5.8	15.8	34	66
3 h	38.4	40.2	5.6	15.8	34	66

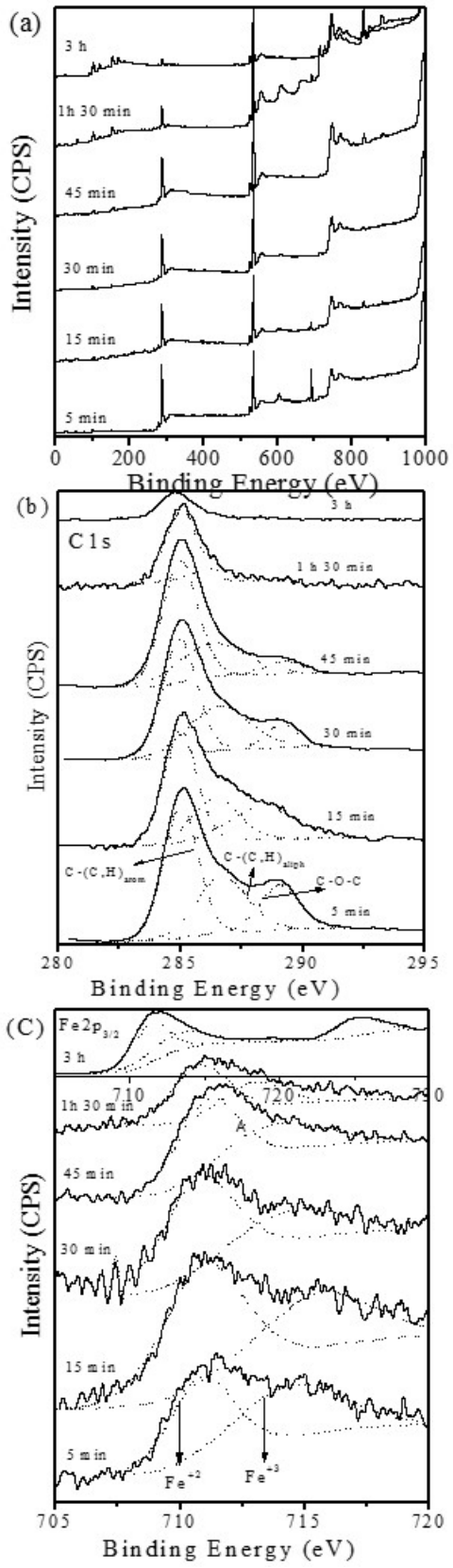

Figure 6. XPS (a) survey (b) C1s and (c) Fe2p spectra for different UVO exposure time.

3.3. Mechanism of iron oxide formation and wettability. The water contact angles were also measured to investigate changes in surface chemistry. The contact angle for the phase separated BCP film is 74° which increased to 96° after the ethanol treatment presumably due to removal of the more hydrophilic PEO component making the surface more hydrophobic.[22] When the iron species are infiltrated via ethanol swelling of the PEO block, the iron species are thought to be associated with the polar PEO block due to coordination bonds between metal vacant d-orbital and the free electron pairs of O atoms.[10] Iron oxide nanoparticles are formed by simple inclusion of metal ions (in a metal nitrate ethanol solution) into the PEO component by spin coating. Similarly iron oxide nanoparticles can be formed by immersing the BCP template into the precursor-ethanol solution followed by UV/Ozone treatment. Longer time required for the iron ion inclusion compared to spin coating and slight thickness variation also observed as PEO component was swollen by ethanol. The hydrophobic nature of PS excludes any probability of the metal ion inclusion into the PS template, so that the PEO activated sites can be considered as sorbtive cylinders. PEO is known to have good affinity with cations[23] and it is believed that swelling of PEO by ethanol allows rapid incorporation of the metal cations or perhaps colloidal entities into these active cylinders. The mechanism of cation ($Fe^{2+/3+}$) inclusion is probably via either intra- or intermolecular coordination via electron donation from the PEO block oxygen atoms as shown below.

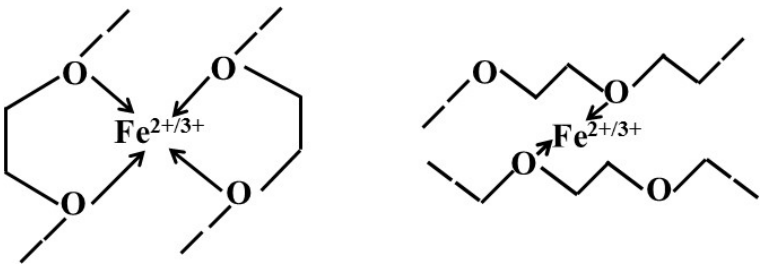

The contact angle decreases to 82° probably due to swelling of the PEO. The contact angle measured for the UVO exposure time of 5, 10, 15, 20, 25 and 30 min show continued decrease

from 80° to 74°, 72°, 70°, 69° and 68° respectively (Figure 7). This is consistent with known surface chemistry of UVO-polymer surface chemistry and is caused by oxidation and insertion of oxygen-containing functional groups (from atomic oxygen formed by the UV irradiation) such as hydroxyl (C-OH) and carboxylic (O-C=O) groups into the polymer chain.[18, 24] This breaks the C-C bonds and helps remove the polymer. It was also reported that a time limit of > 100 sec is required for the UV light and ozone gas collectively affects the polymer surface.[25] Particularly, within 10 minutes of exposure time creates more functional groups than prolonged UVO exposure which results morphological changes accompanied with surface roughening through dissociation or etching of the polymers.[24] The kinetics of this process is complex because the oxidation is intermediate to removal of the polymer as CO_2. Note that the contact angle changes little after the 15 minute UVO treatment suggesting the surface chemistry is constant after this period. However, the corresponding C1s signal which continues to decrease shows carbon is still present. Indeed, this only reaches a constant level (due to adventitious carbon presence) after an hour when the O1s signal starts to rise (Figure 6a). This suggests that this is more difficult to remove carbonaceous layer formed through oxidation and crosslinking of carbon species. The formation of this robust layer may form a template for nanodot formation ensuring only limited growth and migration of iron materials. To confirm this, the iron species load BCP template was exposed to UVO for different time period followed by air calcination at 800° C. It was found that at least 15 minutes of UVO exposure followed by annealing at 800° C for at least 30 minutes was needed to create stable iron oxide nanopatterns by this combined method. But it was reported that calcination leads to a phase change of the iron oxides from Fe_3O_4 to hematite Fe_2O_3.[12] Heating also causes reduction in the average diameter and height consistent with high temperature densification. Shorter exposure times effectively led to very little ordered nanodot formation indicating that the polymer template is not sufficiently robust to act as an effective template. These data very strongly

suggest that the formation of the particles occurs after the initial reaction of the polymer film. We assert that the UV light used has two effects. Firstly, it is absorbed by atmospheric oxygen and leads to generation of ozone that brings about oxidation (and removal of polymer).[26] It also has a strong polystyrene crosslinking effect which is responsible for cross-linking and forming an effective template.[27] Note that the ozone concentrations within the chamber had not been measured. But the distance between the samples and UV source was kept constant for all the experiments results same concentrations of ozone formation.

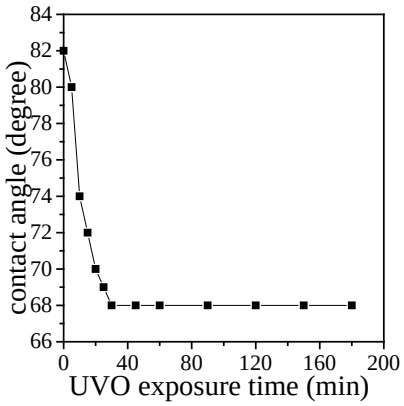

Figure 7. Variation of water contact angle with UVO exposure time.

4. CONCLUSION

A mechanism for solvent mediated metal ion insertion into a BCP film can be proposed and is described in Scheme 1. Solvent annealing of the spin coated film in toluene produces hexagonally arranged PEO cylinders perpendicular to the substrate in PS matrix (Scheme 1A). Modification of PEO domains creates ‘nanoporous’ template (Scheme 1B) onto which an iron nitrate-ethanol solution was spin coated which resulted in inclusion of the iron ions into the PEO domain (Scheme 1C). For 5 minutes UVO time, ordered nanopatterns were still observed

with a minimal film thickness decrease due to small levels of polymer removal as depicted in Scheme 1D. This may be when the PS cross-linking occurs. For UVO times of 15, 30 and 60 mins the polymer removal rate increases and the surface roughens and the film thickness reduces considerable (Scheme 1E-G). Eventually polymer free iron oxide nanoparticle patterns were formed after 2h (Scheme 1H).

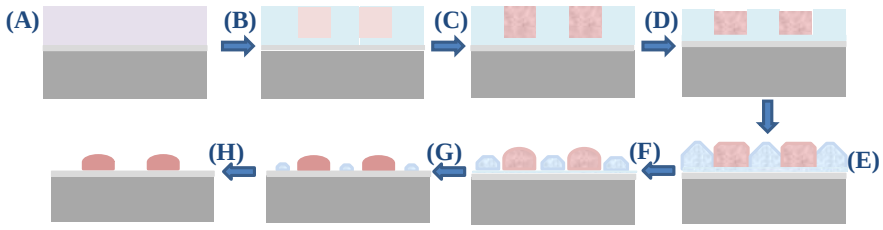

Scheme 1 Process of formation of iron oxide nanoparticle arrays through this BCP inclusion process concerning different stages with UVO time.

This paper gives an in-depth view of the necessity of UVO processing step for the generation of iron oxide materials nanopattern without pattern damage through BCP inclusion technique. Hexagonally arranged self-assembled PS-b-PEO nanopatterns with perpendicularly oriented PEO cylinders inside PS matrix was realized by a simple solvent annealing process. The BCP template for the generation of iron oxides was created by an effective ethanol treatment which etch and/or modification of the PEO domains. Spin coating the precursor ethanolic solution followed by UVO treatment creates well-ordered, stable iron oxide nanopatterns mimic the original self-assembled BCP pattern. Strong coordination bond between metallic ions and free electron pairs of O atoms of the precursor solution is responsible for the inclusion of metals within the BCP template. The UVO treatment leads to cross-link the BCP, formation of iron oxides and removal of polymers simultaneously. A shorter time of 15 minutes of UVO treatment is required followed by calcinations to generate similar patterns. The loss of polymer

via reaction with atomic oxygen and ozone molecules to create C-O and C=O moieties and eventual formation of CO_2(g). These reactions appear to be catalyzed by the metal. The precursor is oxidized and nanoparticles form at the interface of the substrate and the film. These grow with time, exceeding the cylinder domain size due presumably to transport across the surface of the particle as it forms. This also results morphological change accompanied with surface roughening through dissociation or etching of the polymers with time. Combined effect of UV light and ozone gas is necessary for the iron oxide nanopattern formation.

AUTHOR INFORMATION

Corresponding Authors

*Email: morrism2@tcd.ie; g_tandra@yahoo.co.in

Notes

The authors declare no competing financial interest.

ACKNOWLEDGEMENTS

We acknowledge financial support from the Science Foundation Ireland AMBER grant 12/RC/2278 and Science Foundation Ireland Industry Fellowship Programme 15/IFB/3626. We also thank Ryan Enright, Bell labs and NOKIA(IE) for the industrial assistance. We would also like to thank Dr. Michael Schmidt and Dr. Eoin K. McCarthy for the TEM assistance.

Data Availability: The raw data required to reproduce these findings are available to download from www.sciencedirect.com. The processed data required to reproduce these findings are available to download from www.sciencedirect.com.

REFERENCES

1. Fan, H. J.; Werner, P.; Zacharias, M. Semiconductor Nanowires: From Self-Organization to Patterned Growth. *Small* **2006,** *2*, 700-717.

2. Henzie, J.; Barton, J. E.; Stender, C. L.; Odom, T. W. Large-Area Nanoscale Patterning: Chemistry Meets Fabrication. *Accounts Chem. Res.* **2006,** *39,* 249-257.

3. Nie, Z. H.; Kumacheva, E. Patterning Surfaces with Functional Polymers. *Nat. Mater.* **2008,** *7*, 277-290.

4. Liu, J. F.; Miller, G. P. Field-Assisted Nanopatterning of Metals, Metal Oxides and Metal Salts. *Nanotechnology* **2009,** *20*.

5. Nunns, A.; Gwyther, J.; Manners, I. Inorganic Block Copolymer Lithography. *Polymer* **2013,** *54*, 1269-1284.

6. Mun, J. H.; Cha, S. K.; Kim, H.; Moon, H. S.; Kim, J. Y.; Jin, H. M.; Choi, Y. J.; Baek, J. E.; Shin, J.; Kim, S. O. Nanodomain Swelling Block Copolymer Lithography for Morphology Tunable Metal Nanopatterning. *Small* **2014,** *10*, 3742-3749.

7. Kim, S. H.; Park, O. H.; Nederberg, F.; Topuria, T.; Krupp, L. E.; Kim, H. C.; Waymouth, R. M.; Hedrick, J. L. Application of Block-Copolymer Supramolecular Assembly for the Fabrication of Complex Tio2 Nanostructures. *Small* **2008,** *4*, 2162-2165.

8. Haryono, A.; Binder, W. H. Controlled Arrangement of Nanoparticle Arrays in Block-Copolymer Domains. *Small* **2006,** *2*, 600-611.

9. Jung, Y. S.; Ross, C. A. Well-Ordered Thin-Film Nanopore Arrays Formed Using a Block-Copolymer Template. *Small* **2009,** *5*, 1654-1659.

10. Faustini, M.; Grosso, D. Self-Assembled Inorganic Nanopatterns (Inps) Made by Sol-Gel Dip-Coating: Applications in Nanotechnology and Nanofabrication. *C. R. Chim.* **2016,** *19*, 248-265.

11. Ghoshal, T.; Fleming, P. G.; Holmes, J. D.; Morris, M. A. The Stability of ‘‘Ce2o3’’ Nanodots in Ambient Conditions: A Study Using Block Copolymer Templated Structures. *J. Mater. Chem.* **2012,** *22*, 22949-22957.

12. Ghoshal, T.; Maity, T.; Godsell, J. F.; Roy, S.; Morris, M. A. Large Scale Monodisperse Hexagonal Arrays of Superparamagnetic Iron Oxides Nanodots: A Facile Block Copolymer Inclusion Method. *Adv. Mater.* **2012,** *24*, 2390-2397.

13. Ghoshal, T.; Ntaras, C.; O'Connell, J.; Shaw, M. T.; Holmes, J. D.; Avgeropoulos, A.; Morris, M. A. Fabrication of Ultra-Dense Sub-10 Nm in-Plane Si Nanowire Arrays by Using a Novel Block Copolymer Method: Optical Properties. *Nanoscale* **2016,** *8*, 2177-2187.

14. Ghoshal, T.; Senthamaraikannan, R.; Shaw, M. T.; Holmes, J. D.; Morris, M. A. Fabrication of Ordered, Large Scale, Horizontally-Aligned Si Nanowire Arrays Based on an in Situ Hard Mask Block Copolymer Approach. *Adv. Mater.* **2014,** *26*, 1207-1216.

15. Ghoshal, T.; Shaw, M. T.; Bolger, C. T.; Holmes, J. D.; Morris, M. A. A General Method for Controlled Nanopatterning of Oxide Dots: A Microphase Separated Block Copolymer Platform. *J. Mater. Chem.* **2012,** *22*, 12083-12089.

16. Ghoshal, T. M., T; Senthamaraikannan, R; Shaw, M; Carolan, P; Holmes, J; Roy, S; Morris, M Size and Space Controlled Hexagonal Arrays of Superparamagnetic Iron Oxide Nanodots: Magnetic Studies and Application. *Scientific Reports* **2013,** *3*, 2772.

17. Ouyang, M.; Yuan, C.; Muisener, R. J.; Boulares, A.; Koberstein, J. T. Conversion of Some Siloxane Polymers to Silicon Oxide by Uv/Ozone Photochemical Processes. *Chem. Mat.* **2000,** *12*, 1591-1596.

18. Teare, D. O. H.; Ton-That, C.; Bradley, R. H. Surface Characterization and Ageing of Ultraviolet-Ozone-Treated Polymers Using Atomic Force Microscopy and X-Ray Photoelectron Spectroscopy. *Surf. Interface Anal.* **2000,** *29*, 276-283.

19. do Rego, A. M. B.; Pellegrino, O.; Martinho, J. G.; da Silva, J. L. Diblock Copolymer Ultrathin Films Studied by High Resolution Electron Energy Loss Spectroscopy. *Surf. Sci.* **2001,** *482*, 1228-1234.

20. Sardella, E.; Gristina, R.; Senesi, G. S.; d'Agostino, R.; Favia, P. Homogeneous and Micro-Patterned Plasma-Deposited Peo-Like Coatings for Biomedical Surfaces. *Plasma Process. Polym.* **2004,** *1*, 63-72.

21. Prakash, R.; Choudhary, R. J.; Chandra, L. S. S.; Lakshmi, N.; Phase, D. M. Electrical and Magnetic Transport Properties of Fe3o4 Thin Films on a Gaas(100) Substrate. *J. Phys.-Condes. Matter* **2007,** *19*.

22. Faghihnejad, A.; Zeng, H. B. Interaction Mechanism between Hydrophobic and Hydrophilic Surfaces: Using Polystyrene and Mica as a Model System. *Langmuir* **2013,** *29*, 12443-12451.

23. Tsvetanov, C. B.; Stamenova, R.; Dotcheva, D.; Doytcheva, M.; Belcheva, N.; Smid, J. Intelligent Networks Based on Poly(Oxyethylene). *Macromol. Symp.* **1998,** *128*, 165-182.

24. Sham, M. L.; Li, J.; Ma, P. C.; Kim, J. K. Cleaning and Functionalization of Polymer Surfaces and Nanoscale Carbon Fillers by Uv/Ozone Treatment: A Review. *J. Compos Mater.* **2009,** *43*, 1537-1564.

25. Kuang, P.; Lee, J. H.; Kim, C. H.; Ho, K. M.; Constant, K. Improved Surface Wettability of Polyurethane Films by Ultraviolet Ozone Treatment. *J. Appl. Polym. Sci.* **2010,** *118*, 3024-3033.

26. Vig, J. R. Uv Ozone Cleaning of Surfaces. *J. Vac. Sci. Technol. A-Vac. Surf. Films* **1985,** *3*, 1027-1034.

27. Palacios, M.; Garcia, O.; Rodriguez-Hernandez, J. Constructing Robust and Functional Micropatterns on Polystyrene Surfaces by Using Deep Uv Irradiation. *Langmuir* **2013,** *29*, 2756-2763.